MATERIALS SCIENCE

Ultrathin graphdiyne film on graphene through solution-phase van der Waals epitaxy

Xin Gao[1]*, Yihan Zhu[2]*, Ding Yi[3], Jingyuan Zhou[1], Shishu Zhang[1], Chen Yin[1], Feng Ding[3], Shuqing Zhang[1], Xiaohui Yi[4], Jizheng Wang[4], Lianming Tong[1†], Yu Han[5†], Zhongfan Liu[1†], Jin Zhang[1†]

Graphdiyne (GDY) is an ordered two-dimensional (2D) carbon allotrope comprising sp- and sp^2-hybridized carbon atoms with high degrees of π-conjugation, which features a natural band gap and superior electric properties. However, the synthesis of one- or few-layer GDY remains challenging because of the free rotation around alkyne-aryl single bonds and the lack of thickness control. We report the facile synthesis of an ultrathin single-crystalline GDY film on graphene through a solution-phase van der Waals epitaxial strategy. The weak admolecule-substrate interaction at the heterojunction drastically relaxes the large lattice mismatch between GDY and graphene. It allows the fast in-plane coupling of admolecules and slow out-of-plane growth toward the formation of an incommensurately stacked heterostructure, which is composed of single-layer graphene and few-layer ABC-stacked GDY, as directly observed by electron microscopy and identified from Raman fingerprints. This study provides a general route not only to the bottom-up synthesis of intriguing 2D acetylenic carbon allotropes but also to the device fabrication for the direct measurement of their intrinsic electrical, mechanical, and thermal properties.

INTRODUCTION

The exploitation of low-dimensional carbon allotropes has long been a research topic of particular interest because of their fascinating properties and outstanding performance in diverse fields. The discovery of fullerenes [zero-dimensional (0D)] (*1*), carbon nanotubes (1D) (*2*), and graphene (2D) (*3*) as typical low-dimensional carbon allotropes with similar chemical scaffolds containing sp^2-hybridized carbon has reached great success because of their unprecedented electrical, mechanical, and thermal properties. In 1997, Haley *et al.* (*4*) proposed a unique 2D carbon allotrope with a totally different chemical scaffold combining both sp- and sp^2-hybridized carbon, namely, graphdiyne (GDY). The presence of acetylenic linkages endows GDY with distinct physical and chemical properties from sp^2-hybridized carbon allotropes (*5*). For example, GDY exhibits a predicted natural moderate band gap of 0.44 to 1.47 eV while maintaining a high carrier mobility of 10^4 to 10^5 $cm^2 V^{-1} s^{-1}$ at room temperature (*6*–*13*). In addition, the highly π-conjugated structure and the ordered porous topology enable its great potential in applications such as catalysis (*14*), gas separation (*12*), and energy-related fields (*15*, *16*).

Encouraged by these intriguing properties of GDY, tremendous efforts have been made to experimentally synthesize such 2D acetylenic carbon allotropes. For example, dry chemistry approaches have been used, but only noncovalent assemblies or oligomers are derived on the metal surface under ultrahigh vacuum (*17*, *18*). In contrast, the wet chemistry approach achieved the scalable synthesis of GDY and further improved the quality of GDY. Li *et al.* (*19*) conducted a pioneering work in preparing a uniform GDY film with ~1-μm thickness via Glaser coupling reaction in solution, where copper foil was used as both the catalyst and the substrate. Following this work, several studies have been carried out to further control the growth of GDY. Zhou *et al.* (*20*) reported a feasible synthetic route of GDY nanowalls by using a modified Glaser-Hay coupling. Different morphologies of GDY on various substrates were also prepared by using anodic aluminum oxide template (*21*) and copper envelop strategy (*22*). Multilayer GDY nanosheets were prepared via a successive alkyne-alkyne homocoupling reaction at the interface between monomer/catalyst solutions (*23*). More recently, we proposed a template-assisted approach for synthesis of thin-film GDY (3 to 20 nm) by using Hiyama coupling reaction at 65° to 70°C (*24*). Despite the promising advances in pursuing high-quality GDY, the synthesis of a single-crystalline GDY film thin enough to retain its "2D character" (that is, typically one- to few-layer) is, however, very challenging. The major obstacle lies in the fact that (i) the free rotation around alkyne-aryl single bonds in monomers usually leads to a highly branched or cross-linked framework with less ordering rather than the desired crystalline planar framework of GDY during polymerization; (ii) conventional epitaxial growth requires severe lattice matching conditions between the epilayer and the substrate with dangling bonds due to their strong interaction; and (iii) the step-down diffusion of monomers adsorbed on the epilayers is hindered by the Ehrlich-Schwoebel (ES) barrier (*25*), which thus leads to the accumulation and nucleation of admolecules on the epilayer and results in a large thickness via layer-by-layer out-of-plane growth.

Van der Waals (vdW) epitaxy, on the other side, greatly alleviates the lattice matching conditions due to the weak vdW-type interaction between the epilayer and the substrate with saturated surface bonds. The weak binding between the epilayer and admolecules largely promotes the in-plane versus out-of-plane growth of the epilayer by effectively diminishing the ES barrier. In addition, by using substrates with a 2D structure like graphene, its atomically flat surface favors the in-plane coupling rather than out-of-plane cross-linking of admolecules that usually adopt a flat-lying adsorption geometry (*26*). Here, we developed a facile solution-phase vdW epitaxial strategy to confine the GDY growth on graphene by Eglinton reaction using hexaethynylbenzene

[1]Center for Nanochemistry, Beijing Science and Engineering Center for Nanocarbons, Beijing National Laboratory for Molecular Sciences (BNLMS), College of Chemistry and Molecular Engineering, Peking University, Beijing 100871, China. [2]Department of Chemical Engineering, Zhejiang University of Technology, Hangzhou 310014, China. [3]Center for Multidimensional Carbon Materials, Institute for Basic Science, and School of Materials Science and Engineering, Ulsan National Institute of Science and Technology, Ulsan 44919, Republic of Korea. [4]BNLMS, Key Laboratory of Organic Solids, Institute of Chemistry, Chinese Academy of Sciences, Beijing 100871, China. [5]Advanced Membranes and Porous Materials Center, Physical Sciences and Engineering Division, King Abdullah University of Science and Technology, Thuwal 23955-6900, Saudi Arabia.
*These authors contributed equally to this work.
†Corresponding author. Email: jinzhang@pku.edu.cn (J.Z.); zfliu@pku.edu.cn (Z.L.); yu.han@kaust.edu.sa (Y.H.); tonglm@pku.edu.cn (L.T.)

(HEB) as monomers, which can occur at room temperature even with a low monomer concentration. Benefiting from the higher binding energy of HEB monomers on graphene than GDY (1.47 eV versus 0.896 eV, as calculated), the monomers also thermodynamically prefer to adsorb on graphene toward the in-plane Eglinton coupling reaction, especially at low coverage. Together, a much faster in-plane than out-of-plane growth of GDY is expected on graphene through vdW epitaxy. Using this method, we achieved an ultrathin single-crystalline GDY film on graphene, which exhibits excellent electric properties for diverse applications, such as gas sensing. The proposed solution-phase vdW epitaxial strategy here may advance the design of novel 2D acetylenic carbon allotropes with unique structural and physical properties.

RESULTS AND DISCUSSION

Figure 1 (A and B) shows a schematic illustration of the synthetic process of an ultrathin single-crystalline GDY film on graphene. First, single-layered graphene was transferred onto a SiO_2/Si substrate as the substrate for the synthesis of GDY. The optical image and Raman spectra are shown in fig. S1. The high-resolution transmission electron microscopy (HRTEM) images show typical contrast for monolayer graphene (fig. S2). The as-prepared graphene substrate was immersed in a CH_2Cl_2 solution of HEB monomers, where HEB molecules are adsorbed to graphene. Then, a pyridine solution of copper acetate was added dropwise, serving as the catalyst of acetylenic coupling reaction for the synthesis of GDY. To further control the kinetics of the coupling reaction and avoid the side reactions of HEB oxidation, we adopted a low concentration of both the monomer (0.04 mM) and the catalyst (0.7 mM) for the growth of GDY. After reaction under an argon atmosphere at room temperature for 24 hours, the ultrathin GDY film can be synthesized on the graphene surface. Figure 1 (C and D) shows typical optical microscopy (OM) and scanning electron microscopy (SEM) images of GDY/graphene films. The GDY film on the graphene surface is continuous with a lateral dimension of 50 μm. Atomic force microscopy (AFM) analysis (Fig. 1E) exhibits an ultraflat surface with a thickness of only 1.74 nm, inclusive of monolayer graphene.

In addition, GDY was prepared on the exfoliated graphene with different domains for further thickness evaluation. We measured the thickness of these domains before and after growth of GDY, respectively. The typical AFM image is shown in fig. S3 (A and B). The statistical thickness data of as-grown GDY were extracted from 66 independent domains. The data exhibited a narrow bimodal distribution centered at 1.05 ± 0.02 nm (major) and 2.04 ± 0.04 nm (minor), respectively (fig. S3C). Accordingly, most of the as-grown GDY film was determined to have a trilayer thickness.

The as-grown film was separated from the SiO_2/Si substrate and transferred onto a copper grid by a poly(methyl methacrylate) (PMMA)–assisted transfer method (fig. S4), which was then inspected by TEM (Fig. 2A). Figure S5 shows that the as-grown film is mainly composed of carbon. Apart from the graphene layer, a second layer with

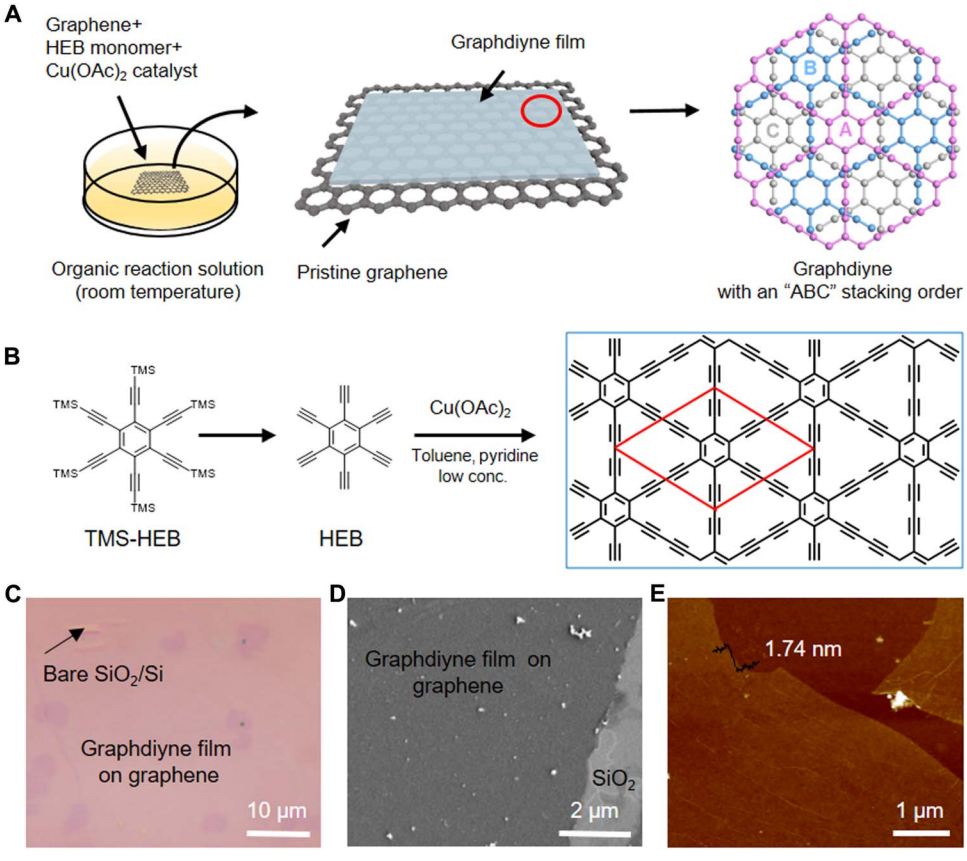

Fig. 1. Synthetic process of single-crystalline GDY on graphene film. (**A**) Schematic illustration of the synthetic process. (**B**) Chemical structure of HEB, hexakis[(trimethylsilyl) ethynyl]benzene (TMS-HEB), and the Eglinton coupling reaction of HEB molecule for the growth of GDY. TMS = $SiMe_3$. Typical OM image (**C**) and SEM image (**D**) of GDY film grown on graphene. (**E**) Typical AFM image of GDY/graphene film on SiO_2/Si substrate, showing a thickness of ~1.74 nm (including a single-layer graphene).

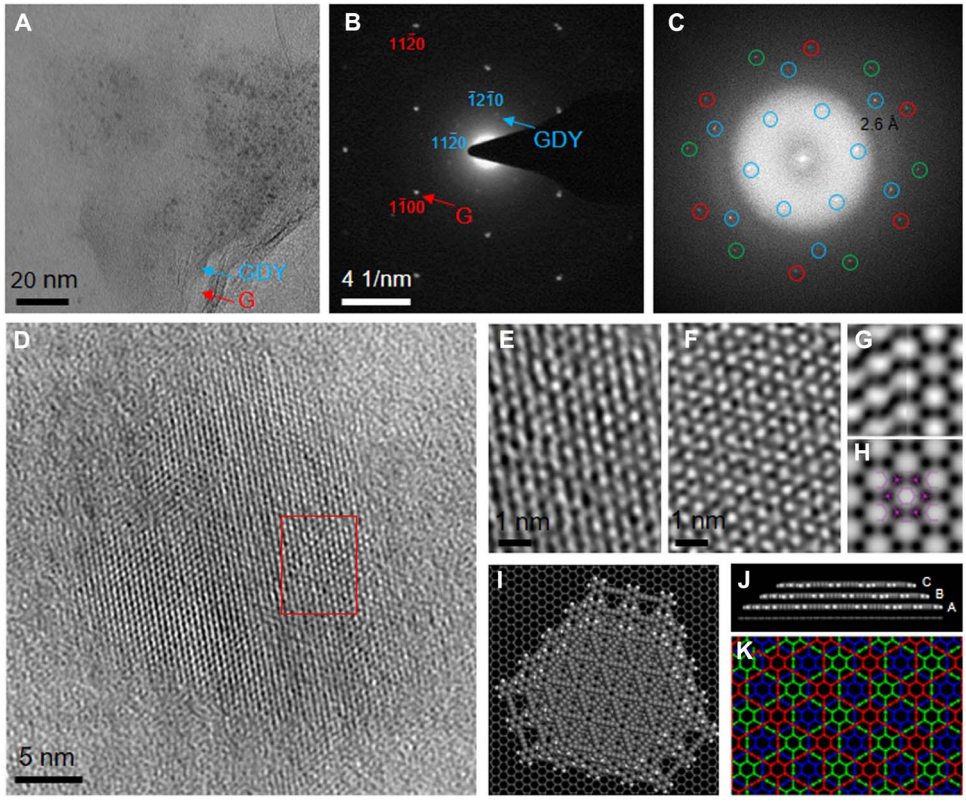

Fig. 2. Aberration-corrected and monochromated HRTEM images of as-synthesized film. (**A**) TEM image of transferred GDY/graphene film on a holey elastic carbon matrix. (**B**) Electron diffraction pattern of as-synthesized film, which shows that GDY and graphene films are both single crystalline. (**C**) Corresponding FFT pattern of HRTEM image. Blue circle, GDY; red and green circles, graphene. (**D**) Aberration-corrected HRTEM imaging of GDY domain. (**E**) Enlarged image in the area highlighted by the red square of Fig. 3D. (**F**) Simulated HRTEM image of GDY with "ABC" stacking mode (amorphous noise included). (**G**) CTF-corrected, lattice-averaged (left) and *p6m* symmetry-imposed images (right). (**H**) Simulated projected potential map with a point spread function width of 2.6 Å. ABC stacking trilayer GDY model embedded. (**I** and **J**) Energetically preferred geometry of vdW heterostructure made of single-layer graphene and ABC-stacked trilayer GDY flake, optimized by self-consistent charge density functional tight-binding methods with dispersion. (**K**) Schematic illustration of GDY with ABC stacking mode.

dark contrast was observed by TEM. The dual-layer structure was more clearly visualized from the edges, as marked in Fig. 2A. Electron diffraction pattern of such transferred film exhibits two sets of overlapping single-crystal diffractions spots, one of which has smaller d spacings (that is, 0.214 and 0.124 nm) and can be easily indexed by the $(1\bar{1}00)$ and $(11\bar{2}0)$ reflections of graphene, respectively (Fig. 2B). The thickness of graphene was further confirmed to be single-layer due to the more intensive $(1\bar{1}00)$ reflections than $(11\bar{2}0)$ reflections. Another set of hexagonally arranged diffraction spots with a larger d spacing of 0.470 nm was observed, which can be indexed by the $(11\bar{2}0)$ reflections of GDY (*23*). Apparently, the dual-layer heterostructure is composed of incommensurately stacked single-crystalline graphene and GDY, which follows the vdW epitaxy growth mode and allows a nearly complete relaxation of large lattice mismatch at the heterointerface. As-grown GDY is oriented with a ~14° interlayer rotation with respect to the underlying graphene, which has also been theoretically predicted to be an energetically preferred vdW heterostructure, as shown in Fig. 2 (I and J). Notably, the $(1\bar{1}00)$ reflections of as-grown GDY are absent, which contradicts with either monolayer, AA-stacked, or AB-stacked GDY structural models with *P6/mmm*, *P6/mmm*, or $P6_3/mmc$ symmetries, respectively (fig. S6). Among all stacking modes of GDY structures with high symmetry, the observed systematic extinction corresponds to rhombohedral (R)–centering and the ABC stacking mode with an R-3m symmetry, as similarly observed in multilayer GDY (*23*, *27*). This is verified by the fact that theoretically predicted ABC-stacked GDY has slightly lower energy than other stacking modes (fig. S7). We were able to directly observe the as-grown GDY/graphene vdW heterostructure at high resolution by using aberration-corrected and monochromated TEM under low voltage (80 kV) and low dose while maintaining its structural integrity (fig. S8). Despite the fact that the amorphous (PMMA) layer used for transferring the GDY/graphene film cannot be completely removed, hexagonal honeycomb lattice contrast with a nearest neighbor distance of ~0.53 nm for bright dots is unambiguously observed, which could be attributed to the highly crystalline ABC-stacked GDY sheets, as schematically shown in Fig. 2K. This point is further confirmed by the good agreement between the experimental HRTEM image of as-grown GDY and the simulated one using an ABC-stacked GDY model, as shown in Fig. 2 (E and F). The GDY/graphene vdW heterostructure can be more clearly identified from the fast Fourier transform (FFT) of the HRTEM image in Fig. 2C, where two sets of reflections belonging to randomly stacked graphene bilayers, as well as another set of reflections for the GDY film, are discriminated from each other. The FFT contains structural information of GDY transferred up to 2.6 Å, with which the contrast transfer function (CTF)–corrected and lattice-averaged (symmetry-imposed) images resolve two neighboring motifs composed of superimposed acetylenic groups and match the simulated potential map of ABC-stacked GDY very well in Fig. 2 (G and H) (*28*). Systematic extinction arising from the R-centering of the ABC-stacked

GDY is also identified in the FFT, and the measured interlayer rotation angle between GDY and one of the graphene layers is ~16°, all of which are consistent with previous observations.

The electronic structure of the as-grown GDY was probed by x-ray photoelectron spectroscopy (XPS), electron energy-loss spectroscopy (EELS), and photoluminescence (PL) spectroscopy, respectively. Figure 3A presents a high-resolution asymmetric C 1s XPS spectrum of the GDY/graphene film. The C 1s peak can be deconvoluted into four subpeaks at 284.6, 285.3, 286.9, and 288.5 eV, corresponding to C–C (sp^2), C–C (sp), C–O, and C=O, respectively (*19*). According to the GDY structural model, the benzene rings are connected to each other by conjugated diyne linkers. The ratio of the sp- to sp^2-hybridized carbon atoms should thus be exactly 2. The experimentally observed ratio is, however, less than 2, owing to the contribution from the underlying graphene fully with sp^2-hybridized carbon. The small amounts of C=O species may originate from traces of impurities or defects in the sample. Moreover, the sp^2- and sp-hybridized carbon in the as-grown film were also identified at nanoscale using site-specific EELS by showing two distinct π* resonance features located at 285.9 and 287.1 eV, respectively (fig. S9). In addition, the PL properties of as-grown GDY were investigated on the hexagonal boron nitride (h-BN) substrate (Fig. 3C and fig. S10). The PL spectrum exhibits a single emission peak, with a maximum at a photon energy of 1.79 eV, which is close to the predicted band gap of GDY (fig. S11).

Raman scattering contains the fingerprint structural information of GDY, especially for those Raman-active diyne linkers arranged in the specific topology of GDY. Although the typical Raman spectra of GDY were systematically studied by group theory and first-principles calculations (*29*), experimentally, the reported Raman spectra always show broadened and poorly resolved bands (*15*, *19*, *23*, *27*), which probably originate from the poor crystallinity and/or highly defective structure and cannot match the predicted spectral features of GDY well. In our experiments, the intrinsic high-resolution Raman fingerprints of GDY were observed by using the graphene substrate via graphene-enhanced Raman scattering (GERS) (*30*), for the first time. Figure 3B shows seven sharp Raman peaks in the range of 1000 to 3000 cm^{-1}, including 1344.8 cm^{-1} (defined as G″), 1430.1 cm^{-1} (defined as G′), 1523.9 cm^{-1} (defined as G), 1586.1 cm^{-1} (defined as G_g), 2105.9 cm^{-1} (defined as Y), 2189.2 cm^{-1} (defined as Y′), and 2696.5 cm^{-1} (defined as $2D_g$). G_g and $2D_g$ bands are assigned to the lattice vibration modes of graphene, as reported (*31*). The remaining Raman bands are from the GDY structure and in agreement with the predicted Raman fingerprints of GDY (fig. S12) (*29*). For example, the Y band (centered at 2105.9 cm^{-1}) and Y′ band (centered at 2189.2 cm^{-1}) are attributed to the in-phase and out-of-phase stretching modes of C≡C triple bonds, respectively, as shown in fig. S13. Polarization-dependent Raman spectra of GDY were further measured in XX (red) and XY (blue) polarization configurations to accurately assign the different vibration modes in GDY (see Materials and Methods). As shown in Fig. 3B, G′ and Y are assigned to the A_{1g} mode, of which the intensity significantly decreases in the XY configuration compared with the XX configuration. In contrast, the E_{2g} modes (G and Y′) are nearly the same in XX (red) and XY (blue) polarization configurations. These results are consistent with the calculated ones using a 2D GDY model (*29*). Notably, compared with HEB monomers, there is an obvious blue shift of Y′ band in the Raman spectra of GDY (fig. S14), likely caused by the coupling reaction of HEB monomers on graphene. The coupling reaction is further confirmed by observing the intensity changes of Y′ band in the in situ Raman spectroscopy experiments of GDY growth (figs. S15 and S16). In addition, the Raman mapping of the Y′-to-$2D_g$ intensity ratio over the marked area further verified the uniformity of as-grown GDY at the macroscopic scale, with a rather uniform contrast shown in Fig. 3 (D to F). The stability of

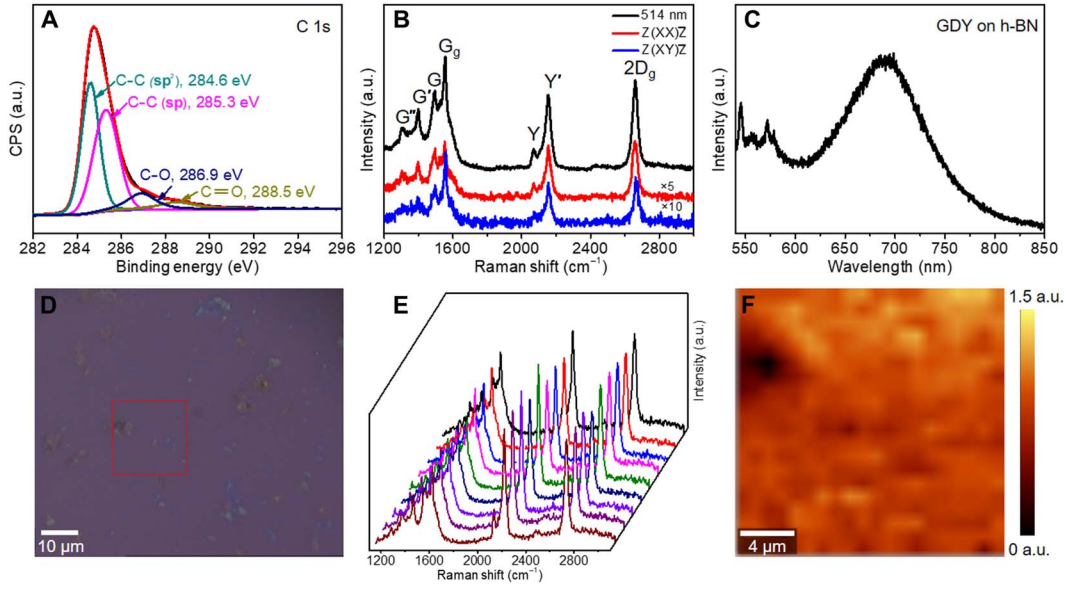

Fig. 3. Spectroscopic characterization of as-grown GDY film. (**A**) High-resolution core-level XPS spectrum of C 1s. CPS, counts per second; a.u., arbitrary units. (**B**) Typical Raman spectrum (black) of GDY grown on graphene transferred to SiO_2/Si substrate and polarization-dependent Raman spectra of GDY measured in XX (red) and XY (blue) polarization configurations by fixing the incident light and the scattered signal's polarization directions in the parallel-polarized configuration and cross-polarized configuration (excitation at 514.5 nm). (**C**) PL spectrum of as-grown GDY on h-BN. (**D**) OM image of as-grown GDY on graphene with a mark indicating the mapping region. (**E**) Typical Raman spectra randomly collected across the corresponding sample in (D). (**F**) Integrated intensity ratio Raman maps of Y band (2189.2 cm^{-1}) and 2D band (2696.5 cm^{-1}) over the marked area in (D), confirming the uniformity of the GDY on the graphene surface in macroscopic scales.

as-prepared GDY on graphene was also investigated by Raman spectroscopy. As shown in fig. S17, after being stored in air for 15 days, the Y′-to-2Dg intensity ratio decreased from ~0.55 to ~0.47, but it was still kept at a high level, exhibiting an air stability.

To provide mechanistic insights into the solution-phase vdW epitaxial growth of GDY, we investigated the Eglinton oxidative homocoupling of HEB monomers both on graphene and in solution. Specifically, GDY was synthesized under the optimized conditions on SiO_2/Si half-covered with single-layer graphene. It is interesting to find that the 2D GDY film would only grow on the surface of graphene rather than that of SiO_2/Si, as observed by Raman spectroscopy and SEM, as shown in Fig. 4 (A and C). The products collected in solution show cross-linked and amorphous structures (Fig. 4B), likely originating from the free rotation around alkyne-aryl single bonds during polymerization. All these results indicate that vdW epitaxial type growth is essential to achieve the ultrathin highly crystalline GDY structures. First-principles calculations propose detailed energetics and kinetics of reaction steps for vdW epitaxy (see Materials and Methods). As shown in fig. S18A, the absorbed HEB molecule shows a flat-lying geometry parallel to the graphene surface with a binding energy of 1.47 eV per molecule. We note that the adsorbed HEB monomers have an energetically preferred rotation angle of ~15° with respect to the underlying graphene in fig. S18 (B and C), which surprisingly coincides with the case of GDY on graphene. Both energy barriers and reaction energies of the vdW epitaxial growth strategy are lower than those of the solution growth strategy, as shown in Fig. 4D and fig. S19. For instance, the energy barrier of the rate-determining step (that is, HEB deprotonation) (steps II to III) of graphene-mediated vdW epitaxy is only 0.174 eV, which is significantly lower than that in solution (0.612 eV). The reduced barrier and the reaction energy are possibly caused by the enhanced interaction between the $Cu(OAc)_2$ catalyst and HEB molecules that are coadsorbed onto the graphene substrate and in the vicinity of each other (Fig. 4E). As a result, the consecutive in-plane coupling of HEB admolecules catalyzed by the coadsorbed $Cu(OAc)_2$ species becomes the fast and energetically favored reaction route that leads to the formation of an ultrathin single-crystalline GDY film (Fig. 4C).

Finally, as a proof-of-concept study of the electrical property and applications of GDY, the GDY/graphene film has been fabricated as an NH_3 gas sensor first, showing great potential in gas sensing (fig. S20). Furthermore, we replace graphene with h-BN for electric measurement. To evaluate the electrical property of the as-synthesized GDY, we fabricated field-effect transistors with SiO_2 as the gate dielectric and conducted the measurement at room temperature. A schematic depiction of the device and *I-V* curve is shown in figs. S21 and S22. The conductivity is calculated as 3180 S m^{-1}, which is comparable with the reported results (*19*, *32*), and demonstrates that our as-prepared GDY film exhibits p-type semiconducting properties.

In summary, we reported a facile synthetic route to ultrathin single-crystalline GDY through a solution-phase vdW epitaxial strategy. The GDY film has a trilayer structure with an ABC stacking order as directly observed by HRTEM. Here, the high quality of the as-synthesized GDY film and the GERS effect ensure that the predicted Raman fingerprints belonging to a perfectly ordered 2D GDY structure are experimentally observed. This study paves the way for the design and synthesis of 2D acetylenic carbon allotropes with different degrees of sp and sp^2 hybridizations by using monomers with diverse structures.

MATERIALS AND METHODS

Preparation of GDY through vdW epitaxy in solution

Chemical vapor deposition–grown graphene was transferred onto a 300-nm SiO_2/Si substrate as the substrate for the synthesis of GDY. The

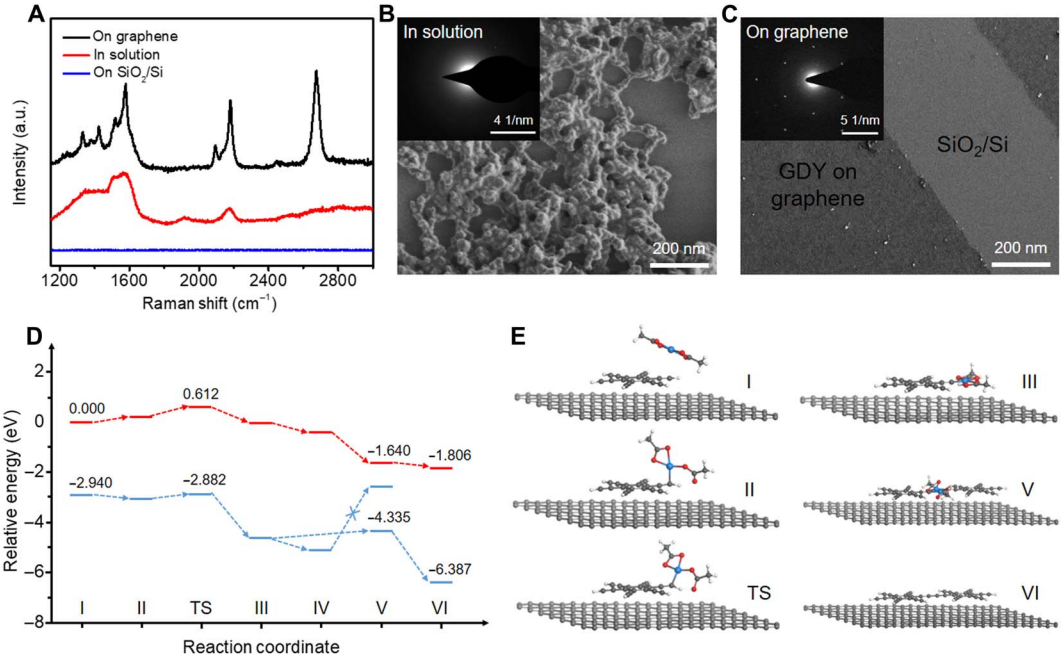

Fig. 4. Proposed mechanism for synthesis of GDY film on graphene through a solution-phase vdW epitaxial strategy. (**A**) Raman spectra of GDY on different reaction areas (on graphene, in solution, and on SiO_2/Si), synthesized under the same conditions. SEM images of as-grown GDY and corresponding selected-area electron diffraction (SAED) pattern in inset, synthesized in solution (**B**) and on graphene (**C**). (**D**) Proposed mechanism for the Eglinton reaction and computed free-energy profiles on graphene (blue) and in solution (red). (**E**) Optimized geometries from I to VI (see fig. S19 for details; Cu, blue; O, red; C, gray, and H, white).

as-prepared graphene substrate was immersed into the dichloromethane solution of HEB (0.1 mM, 5 ml). Then, a pyridine solution (5 ml) of copper acetate (1.6 mM) and toluene (2 ml) were added to the dichloromethane solution of HEB. Under an inert argon atmosphere at room temperature, the successive catalytic coupling reaction for 24 hours led to the growth of the 2D covalent network, generating an ultrathin GDY film at the graphene surface. Using the same synthetic procedures, GDY can be synthesized on h-BN by using h-BN as the substrate for the synthesis of GDY. The as-prepared GDY on h-BN was used for PL and the electronic measurement. One- to few-layer graphene samples mechanically exfoliated on a 300-nm SiO_2/Si substrate were also used to synthesize GDY for the thickness analysis.

TEM image processing and simulation

HRTEM images and EELS spectra were taken on an FEI Titan 60-300 electron microscope equipped with a spherical aberration (Cs) corrector in the image-forming (objective) lens and a monochromator, operated under 80 kV. HRTEM simulation was performed by using the multislice method implemented in QSTEM software (*33*). Simulation conditions used were as follows: 80 kV; Cs = 10 μm; Cc = 1 mm; ΔE = 0.13 eV; Δf = 68 nm; α = 0.2 mrad; focal spread = 5 nm; an objective aperture was used.

Polarized Raman measurement

Polarized Raman spectra were measured using JY Horiba HR800 with a 514.5 nm laser. The optical layout is shown in fig. S23. The incident polarization direction was determined by polarizer I, and polarizer II was in front of the detector. The Z(XX)Z and Z(XY)Z configurations can be obtained by changing the relative angle between the polarization direction of the polarizers. GDY belongs to the D_{6h} point group, and the phonon modes at the Brillouin zone center can be presented as

$$\Gamma_{\text{graphdiyne}} = 2A_{2u} + 5E_{1u} + 3B_{1u} + 3B_{2u} + 3E_{2u} + 3A_{1g} + 3A_{2g} + 3B_{1g} + 3E_{1g} + 6E_{2g}$$

A_{1g}, E_{1g}, and E_{2g} modes are Raman-active under backscattering geometry, but E_{1g} modes cannot be detected.

The Raman tensors of the A_{1g} and E_{2g} modes can be presented as follows

$$R(A_{1g}) = \begin{pmatrix} a & 0 & 0 \\ 0 & a & 0 \\ 0 & 0 & b \end{pmatrix}$$

$$R(E_{2g}) = \begin{pmatrix} 0 & d & 0 \\ d & 0 & 0 \\ 0 & 0 & 0 \end{pmatrix} \cdot \begin{pmatrix} d & 0 & 0 \\ 0 & -d & 0 \\ 0 & 0 & 0 \end{pmatrix}$$

For A_{1g} modes, under the XX configuration, the Raman intensity can be calculated as

$$I_{xx} = \left| \begin{pmatrix} 1 & 0 & 0 \end{pmatrix} \cdot \begin{pmatrix} a & 0 & 0 \\ 0 & a & 0 \\ 0 & 0 & b \end{pmatrix} \cdot \begin{pmatrix} 1 \\ 0 \\ 0 \end{pmatrix} \right|^2 = a^2$$

while under the XY configuration, the Raman intensity is zero. For E_{2g} modes, under XX and XY configurations, the Raman intensities are d^2. With polarized Raman spectra, the Raman modes can be assigned.

Free-energy computation during the synthesis of GDY

First-principles calculations were performed using the density functional theory method implemented in the Vienna Ab-initio Simulation Package code to obtain the energy variation during the synthesis of GDY. The generalized gradient approximation with the Perdew-Burke-Ernzerhof–type exchange-correlation functional and the projector augmented wave method were adopted in all calculations, as well as the Tkatchenko-Scheffler (TS) method for the vdW corrections. Spin-polarized calculations were considered for all models. The plane-wave energy cutoff was fixed at 400 eV. The climbing image nudged elastic band (cNEB) method was exploited to locate the transition states during the process of deprotonation. The convergence of energy and force was set as 10^{-4} and 10^{-2} eV/Å (0.05 eV/Å for cNEB calculations), respectively.

SUPPLEMENTARY MATERIALS

Supplementary material for this article is available at http://advances.sciencemag.org/cgi/content/full/4/7/eaat6378/DC1

Supplementary Materials and Methods

Fig. S1. Optical image and corresponding Raman spectrum of graphene film on SiO_2/Si substrate.

Fig. S2. HRTEM image of graphene substrate.

Fig. S3. Thickness analysis of as-grown GDY on graphene through a solution-phase vdW epitaxial strategy.

Fig. S4. The transfer process of the as-prepared GDY/graphene film from SiO_2/Si substrate to copper grid.

Fig. S5. Scanning TEM image and energy-dispersive x-ray spectroscopy elemental mapping images of C, O, and Si for GDY/graphene.

Fig. S6. GDY models with AA, AB, and ABC stacking modes and corresponding simulated SAED patterns of the stacking models.

Fig. S7. Calculated optimal binding energy of AA-, AB-, and ABC-stacked GDY structural models.

Fig. S8. As-grown GDY/graphene vdW heterostructure at high resolution.

Fig. S9. Monochromated core-loss EELS spectra of GDY/graphene film collected under the (low-loss and core-loss) dual EELS mode.

Fig. S10. Raman spectrum of GDY grown on h-BN substrate.

Fig. S11. Hybrid functional HSE06 predicted band structures and band gaps (Eg) for monolayer, bilayer, and trilayer GDY.

Fig. S12. Typical Raman spectra of GDY grown on graphene (red) with a reference blank graphene on SiO_2/Si substrate (black) and the calculated Raman spectra (*29*) of GDY (blue).

Fig. S13. Raman spectrum and corresponding vibrational modes of GDY.

Fig. S14. Raman spectra of HEB monomer (blue), TMS-HEB monomer (black), and GDY (red).

Fig. S15. In situ Raman spectroscopy to detect the change of the Y′ peak in GDY, which is a Raman-active peak from the stretching of C≡C triple bonds.

Fig. S16. The intensity of typical Y′ (2189.0 cm^{-1}) peak as a function of reaction time, using the peak (520.7 cm^{-1}) from Si substrate for intensity normalization.

Fig. S17. Raman spectra taken from the same sample after being stored in air for several days.

Fig. S18. Theoretical simulations of adsorption behavior of HEB on graphene.

Fig. S19. Detailed structures and relative energy of I to VI and TS.

Fig. S20. NH_3 detection at room temperature and atmospheric pressure.

Fig. S21. Evaluation of the electrical property of the as-synthesized GDY.

Fig. S22. OM images of the device in fig. S20.

Fig. S23. The optical layout of the polarized Raman measurement.

References (*34*–*40*)

REFERENCES AND NOTES

1. H. W. Kroto, J. R. Heath, S. C. O'Brien, R. F. Curl, R. E. Smalley, C_{60}: Buckminsterfullerene. *Nature* **318**, 162–163 (1985).
2. S. Iijima, Helical microtubules of graphitic carbon. *Nature* **354**, 56–58 (1991).
3. K. S. Novoselov, A. K. Geim, S. V. Morozov, D. Jiang, Y. Zhang, S. V. Dubonos, I. V. Grigorieva, A. A. Firsov, Electric field effect in atomically thin carbon films. *Science* **306**, 666–669 (2004).
4. M. M. Haley, S. C. Brand, J. J. Pak, Carbon networks based on dehydrobenzoannulenes: Synthesis of graphdiyne substructures. *Angew. Chem. Int. Ed. Engl.* **36**, 836–838 (1997).

5. Y. Li, L. Xu, H. Liu, Y. Li, Graphdiyne and graphyne: From theoretical predictions to practical construction. *Chem. Soc. Rev.* **43**, 2572–2586 (2014).
6. K. Srinivasu, S. K. Ghosh, Graphyne and graphdiyne: Promising materials for nanoelectronics and energy storage applications. *J. Phys. Chem. C* **116**, 5951–5956 (2012).
7. N. Narita, S. Nagai, S. Suzuki, K. Nakao, Optimized geometries and electronic structures of graphyne and its family. *Phys. Rev. B* **58**, 11009–11014 (1998).
8. A. N. Enyashin, A. L. Ivanovskii, Graphene allotropes. *Phys. Status Solidi B Basic Solid State Phys.* **248**, 1879–1883 (2011).
9. G. Luo, X. Qian, H. Liu, R. Qin, J. Zhou, L. Li, Z. Gao, E. Wang, W.-N. Mei, J. Lu, Y. Li, S. Nagase, Quasiparticle energies and excitonic effects of the two-dimensional carbon allotrope graphdiyne: Theory and experiment. *Phys. Rev. B* **84**, 075439 (2011).
10. M. Long, L. Tang, D. Wang, Y. Li, Z. Shuai, Electronic structure and carrier mobility in graphdiyne sheet and nanoribbons: Theoretical predictions. *ACS Nano* **5**, 2593–2600 (2011).
11. Q. Zheng, G. Luo, Q. Liu, R. Quhe, J. Zheng, K. Tang, Z. Gao, S. Nagase, J. Lu, Structural and electronic properties of bilayer and trilayer graphdiyne. *Nanoscale* **4**, 3990–3996 (2012).
12. Y. Jiao, A. Du, M. Hankel, Z. Zhu, V. Rudolph, S. C. Smith, Graphdiyne: A versatile nanomaterial for electronics and hydrogen purification. *Chem. Commun.* **47**, 11843–11845 (2011).
13. J. He, S. Y. Ma, P. Zhou, C. X. Zhang, C. He, L. Z. Sun, Magnetic properties of single transition-metal atom absorbed graphdiyne and graphyne sheet from DFT + U calculations. *J. Phys. Chem. C* **116**, 26313–26321 (2012).
14. J. Li, X. Gao, B. Liu, Q. Feng, X.-B. Li, M.-Y. Huang, Z. Liu, J. Zhang, C.-H. Tung, L.-Z. Wu, Graphdiyne: A metal-free material as hole transfer layer to fabricate quantum dot-sensitized photocathodes for hydrogen production. *J. Am. Chem. Soc.* **138**, 3954–3957 (2016).
15. H. Shang, Z. Zuo, L. Li, F. Wang, H. Liu, Y. Li, Y. Li, Ultrathin graphdiyne nanosheets grown in situ on copper nanowires and their performance as lithium-ion battery anodes. *Angew. Chem. Int. Ed. Engl.* **57**, 774–778 (2018).
16. Z. Huang, Z. Yu, Y. Li, J. Wang, ZnO ultraviolet photodetector modified with graphdiyne. *Acta Phys. Chim. Sin.* **34**, 1088–1094 (2018).
17. H.-Y. Gao, P. A. Held, S. Amirjalayer, L. Liu, A. Timmer, B. Schirmer, O. D. Arado, H. Mönig, C. Mück-Lichtenfeld, J. Neugebauer, A. Studer, H. Fuchs, Intermolecular on-surface σ-bond metathesis. *J. Am. Chem. Soc.* **139**, 7012–7019 (2017).
18. Q. Sun, L. Cai, H. Ma, C. Yuan, W. Xu, Dehalogenative homocoupling of terminal alkynyl bromides on Au (111): Incorporation of acetylenic scaffolding into surface nanostructures. *ACS Nano* **10**, 7023–7030 (2016).
19. G. Li, Y. Li, H. Liu, Y. Guo, Y. Li, D. Zhu, Architecture of graphdiyne nanoscale films. *Chem. Commun.* **46**, 3256–3258 (2010).
20. J. Zhou, X. Gao, R. Liu, Z. Xie, J. Yang, S. Zhang, G. Zhang, H. Liu, Y. Li, J. Zhang, Z. Liu, Synthesis of graphdiyne nanowalls using acetylenic coupling reaction. *J. Am. Chem. Soc.* **137**, 7596–7599 (2015).
21. G. Li, Y. Li, X. Qian, H. Liu, H. Lin, N. Chen, Y. Li, Construction of tubular molecule aggregations of graphdiyne for highly efficient field emission. *J. Phys. Chem. C* **115**, 2611–2615 (2011).
22. X. Gao, J. Li, R. Du, J. Zhou, M.-Y. Huang, R. Liu, J. Li, Z. Xie, L.-Z. Wu, Z. Liu, J. Zhang, Direct synthesis of graphdiyne nanowalls on arbitrary substrates and its application for photoelectrochemical water splitting cell. *Adv. Mater.* **29**, 1605308 (2017).
23. R. Matsuoka, R. Sakamoto, K. Hoshiko, S. Sasaki, H. Masunaga, K. Nagashio, H. Nishihara, Crystalline graphdiyne nanosheets produced at a gas/liquid or liquid/liquid interface. *J. Am. Chem. Soc.* **139**, 3145–3152 (2017).
24. J. Zhou, Z. Xie, R. Liu, X. Gao, J. Li, Y. Xiong, L. Tong, J. Zhang, Z. Liu, Synthesis of ultrathin graphdiyne film using a surface template. *ACS Appl. Mater. Interfaces* (2018).
25. Y. Nie, C. Liang, P.-R. Cha, L. Colombo, R. M. Wallace, K. Cho, A kinetic Monte Carlo simulation method of van der Waals epitaxy for atomistic nucleation-growth processes of transition metal dichalcogenides. *Sci. Rep.* **7**, 2977 (2017).
26. J. W. Colson, A. R. Woll, A. Mukherjee, M. P. Levendorf, E. L. Spitler, V. B. Shields, M. G. Spencer, J. Park, W. R. Dichtel, Oriented 2D covalent organic framework thin films on single-layer graphene. *Science* **332**, 228–231 (2011).
27. C. Li, X. Lu, Y. Han, S. Tang, Y. Ding, R. Liu, H. Bao, Y. Li, J. Luo, T. Lu, Direct imaging and determination of the crystal structure of six-layered graphdiyne. *Nano Res.* **11**, 1714–1721 (2018).
28. Y. Zhu, J. Ciston, B. Zheng, X. Miao, C. Czarnik, Y. Pan, R. Sougrat, Z. Lai, C.-E. Hsiung, K. Yao, I. Pinnau, M. Pan, Y. Han, Unravelling surface and interfacial structures of a metal–organic framework by transmission electron microscopy. *Nat. Mater.* **16**, 532–536 (2017).
29. S. Zhang, J. Wang, Z. Li, R. Zhao, L. Tong, Z. Liu, J. Zhang, Z. Liu, Raman spectra and corresponding strain effects in graphyne and graphdiyne. *J. Phys. Chem. C* **120**, 10605–10613 (2016).
30. S. Huang, X. Ling, L. Liang, Y. Song, W. Fang, J. Zhang, J. Kong, V. Meunier, M. S. Dresselhaus, Molecular selectivity of graphene-enhanced Raman scattering. *Nano Lett.* **15**, 2892–2901 (2015).
31. C. Neumann, S. Reichardt, P. Venezuela, M. Drögeler, L. Banszerus, M. Schmitz, K. Watanabe, T. Taniguchi, F. Mauri, B. Beschoten, S. V. Rotkin, C. Stampfer, Raman spectroscopy as probe of nanometre-scale strain variations in graphene. *Nat. Commun.* **6**, 8429 (2015).
32. X. Qian, Z. Ning, Y. Li, H. Liu, C. Ouyang, Q. Chen, Y. Li, Construction of graphdiyne nanowires with high-conductivity and mobility. *Dalton Trans.* **41**, 730–733 (2012).
33. C. Koch, "Determination of core structure periodicity and point defect density along dislocations," thesis, Arizona State University (2002).
34. L. Lin, J. Li, H. Ren, A. L. Koh, N. Kang, H. Peng, H. Q. Xu, Z. Liu, Surface engineering of copper foils for growing centimeter-sized single-crystalline graphene. *ACS Nano* **10**, 2922–2929 (2016).
35. G. Kresse, J. Furthmüller, Efficiency of ab-initio total energy calculations for metals and semiconductors using a plane-wave basis set. *Comput. Mater. Sci.* **6**, 15–50 (1996).
36. P. E. Blöchl, Projector augmented-wave method. *Phys. Rev. B* **50**, 17953–17979 (1994).
37. A. Tkatchenko, M. Scheffler, Accurate molecular van der Waals interactions from ground-state electron density and free-atom reference data. *Phys. Rev. Lett.* **102**, 073005 (2009).
38. G. Henkelman, B. P. Uberuaga, H. Jónsson, A climbing image nudged elastic band method for finding saddle points and minimum energy paths. *J. Chem. Phys.* **113**, 9901–9904 (2000).
39. J. Zhong, J. Wang, J.-G. Zhou, B.-H. Mao, C.-H. Liu, H.-B. Liu, Y.-L. Li, T.-K. Sham, X.-H. Sun, S.-D. Wang, Electronic structure of graphdiyne probed by x-ray absorption spectroscopy and scanning transmission x-ray microscopy. *J. Phys. Chem. C* **117**, 5931–5936 (2013).
40. J. Jover, Copper-catalyzed Eglinton oxidative homocoupling of terminal alkynes: A computational study. *J. Chem.* **2015**, 430358 (2015).

Acknowledgments: We thank P. Gao, K. Liu, M. Li, R. Du, Z. Zheng, J. Zhang, B. Deng, H. Ren, and Q. Zhao (all from Peking University, China) for helpful discussions. **Funding:** Y.Z. acknowledges financial support from the Thousand Talents Program for Distinguished Young Scholars and National Natural Science Foundation of China (21771161). This work was supported by the Ministry of Science and Technology of China (2016YFA0200101 and 2016YFA0200104), the National Natural Science Foundation of China (grant nos. 51432002, 51720105003, and 21790052), the Beijing Municipal Science and Technology Project (grant no. Z161100002116026), and the Institute for Basic Science (IBS-R019-D1) of South Korea. **Author contributions:** J. Zhang, Z.L., Y.H., L.T., X.G., and Y.Z. conceived and designed the experiments. X.G., C.Y., and J. Zhou performed the synthesis of samples. Y.Z. and X.G. carried out the TEM image processing, analysis, and simulation. Shishu Zhang was responsible for polarized Raman measurement. X.Y., J.W., and X.G. performed the gas sensor measurement. F.D. and D.Y. performed the theoretical simulations. X.G., Y.Z., F.D., D.Y., Shuqing Zhang, J. Zhang, Z.L., and Y.H. performed the data analysis. X.G. drafted the manuscript, and Y.Z., J. Zhang, Z.L., Y.H., L.T., F.D., D.Y., and S.Z. revised it. All authors commented on the manuscript. **Competing interests:** The authors declare that they have no competing interests. **Data and materials availability:** All data needed to evaluate the conclusions in the paper are present in the paper and/or the Supplementary Materials. Additional data related to this paper may be requested from the authors.

Submitted 21 March 2018
Accepted 23 May 2018
Published 6 July 2018
10.1126/sciadv.aat6378

Citation: X. Gao, Y. Zhu, D. Yi, J. Zhou, S. Zhang, C. Yin, F. Ding, S. Zhang, X. Yi, J. Wang, L. Tong, Y. Han, Z. Liu, J. Zhang, Ultrathin graphdiyne film on graphene through solution-phase van der Waals epitaxy. *Sci. Adv.* **4**, eaat6378 (2018).

Science Advances

Ultrathin graphdiyne film on graphene through solution-phase van der Waals epitaxy

Xin Gao, Yihan Zhu, Ding Yi, Jingyuan Zhou, Shishu Zhang, Chen Yin, Feng Ding, Shuqing Zhang, Xiaohui Yi, Jizheng Wang, Lianming Tong, Yu Han, Zhongfan Liu and Jin Zhang

Sci Adv **4** (7), eaat6378.
DOI: 10.1126/sciadv.aat6378